Optical Properties of Fluid Hydrogen at the Transition to a Conducting State

R. Stewart McWilliams, D. Allen Dalton, Mohammad F. Mahmood, and Alexander F. Goncharov

Phys. Rev. Lett. **116**, 255501 — Published 22 June 2016

DOI: 10.1103/PhysRevLett.116.255501

submitted to Physical Review Letters

TITLE

Optical properties of fluid hydrogen at the transition to a conducting state

AUTHORS

R. Stewart McWilliams,[1,2,3*] D. Allen Dalton,[1] Mohammad F. Mahmood,[1,3]

Alexander F. Goncharov[1,4,5]

AFFILATIONS

[1] Geophysical Laboratory, Carnegie Institution of Washington, 5251 Broad Branch Road NW, Washington DC, 20015, USA

[2] School of Physics and Astronomy and Centre for Science at Extreme Conditions, University of Edinburgh, Peter Guthrie Tait Road, Edinburgh, UK EH9 3FD

[3] Dept. of Mathematics, Howard University, 2400 Sixth Street NW, Washington DC, 20059, USA

[4] Key Laboratory of Materials Physics, Institute of Solid State Physics, Chinese Academy of Sciences, 350 Shushanghu Road, Hefei, Anhui 230031, China

[5] University of Science and Technology of China, Hefei, Anhui 230026, China

SECTION: L7

PACS: 62.50.-p, 81.30.Dz, 78.40.-q, 07.35.+k

ABSTRACT

We use fast transient transmission and emission spectroscopies in the pulse laser heated diamond anvil cell to probe the energy-dependent optical properties of hydrogen at pressures of 10-150 GPa and temperatures up to 6000 K. Hydrogen is absorptive at visible to near-infrared wavelengths above a threshold temperature that decreases from 3000 K at 18 GPa to 1700 K at 110 GPa. Transmission spectra at 2400 K and 141 GPa indicate that the absorptive hydrogen is semiconducting or semi-metallic in character, definitively ruling out a first-order insulator-metal transition in the studied pressure range.

TEXT

Realizing metallic hydrogen and understanding its properties is fundamental for achieving predicted high temperature superconductivity [1], exploring the regime of inertial confinement fusion [2], and resolving the structure and dynamics of giant planetary interiors [3-7]. The metallic state has not been reached yet in the solid at pressures as high as 360 GPa [8-10], but experiments [3,11-16] and theoretical calculations [5,16-27] probing the fluid state at high temperature document an insulator-metal transition (IMT). This fluid metallic state has been theorized to be even the ground state at sufficiently high pressures [19,20], however recent experiments suggest more complex behavior [16,28].

While the underlying physics of metallization in hydrogen is thought to be related to a Mott-like mechanism (band overlap), the essential parts of this phenomenon remain uncaptured because of difficulties in finding appropriate theoretical approximation methods [25-27] and experimental challenges. With increasing pressure, the fluid IMT is expected to exhibit a *critical point* where it

transitions from being continuous to discontinuous (first-order), and merge with the melting line in the limit of high densities [19,20]. Different theoretical studies agree about the transition character, but the location of the critical point varies substantially, with modern estimates ranging as low as 90 GPa [4,5,19,21,22,25-27].

Experiments on fluid hydrogen using shock compression measured gradual increases in electrical conductivity and optical reflectivity to constant, metallic values with increasing temperature and pressure up to 90 GPa [11,13,14], evincing a continuous IMT below this pressure. Between 90 and 140 GPa shock experiments were conducted without direct temperature measurements, leaving the gradual increase and saturation of conductivity detected in this region [3,12,29] open to interpretation: the data are consistent with a continuous IMT [3,12,29] but also show characteristics of a first order IMT naturally broadened by adiabatic compression (e.g. Ref. [30]). Recent isentropic compression measurements suggest the IMT becomes first order by 285 GPa [16], but also assumed temperature, leaving a broad pressure range [3,12,16,29] where the nature of the IMT remains poorly characterized. Static compression, diamond anvil cell (DAC) experiments showed that direct temperature measurements are possible in the metallization regime at high pressure, and detected a fluid phase transition at ~120 GPa, though were not able to provide any characteristics of the transformed state [15].

Hydrogen is a highly reactive and diffusive material, so is challenging to contain in high temperature and pressure experiments for long periods [28,31]. Dynamic compression has probed hydrogen beyond several thousand K at high pressures on microsecond or faster timescales [3,11-14,29], whereas DAC experiments limited to longer timescales reached 1000 and 1800 K using resistive [28] and laser heating [15,31,32], respectively.

In this Letter we describe microsecond, single-pulse laser heating DAC experiments on hydrogen that reach novel conditions not previously characterized by dynamic or static studies (Fig. 1). Time-resolved optical emission and transmission spectroscopy determines sample temperature T and corresponding optical absorptivity α during heat cycles [33,34]. A 4-10 μs long laser pulse heats a metallic (Ir) foil in a hydrogen sample, and heat propagates across the adjacent hydrogen creating a localized heated excited state of several μm in linear dimensions and a few μs long. Transient absorption probing using a continuous laser (CW: 532 nm) and pulsed broadband supercontinuum (BB: 1 MHz, 150 ps, 400-900 nm) was performed by transmission through a hole in the foil at the heated region. Fits of emission spectra to a Planck distribution determined temperature with a time resolution of 0.5-5 μs.

To ensure our measurements probed pristine hydrogen, several precautions were taken. Pressure was measured before and after the heat cycles using Raman spectra of the hydrogen vibron [35] and diamond edge [36], and ruby fluorescence [37]. Vibron signal from the heated area was confirmed before and after heating [34]. Continued heating resulted in decreasing vibron signal, pressure changes (usually but not always negative), decreasing foil hole diameters [34], and occasional anvil fracturing, evincing rapid hydrogen diffusion and loss. Complete loss occurred within ~1 ms of total heating time. Weak Raman lines attributed to Ir hydride [38] appeared in one sample subjected to prolonged heating at high temperature [34], but not in reported experiments.

Upon increasing laser power, time histories of thermal emission during heat cycles exhibited a drastic shift in behavior, similar to that seen in noble gases as a consequence of high-temperature absorption onset [33]. For low peak laser power, the temperature followed the laser power history (Fig. 2a), having a distinct initial peak.

With increasing power, there was a transition to a different thermal response, where temperature did not follow laser power, but instead rose and remained roughly constant, forming a plateau that persisted for an especially long duration (Fig. 3). To examine this transition we performed finite element (FE) models [33,34,39] to investigate how properties of hydrogen samples, such as a temperature-dependent absorption, control temperature history. The lower-temperature behavior is expected for a transparent sample, i.e. where the laser is absorbed entirely in the foil surface. The higher-temperature behavior could not be explained if the sample remained transparent; instead an abrupt increase in sample absorption with temperature (to $\alpha \approx$ 0.1 to 1 μm^{-1}) is needed to reproduce the long temperature plateau, which occurs near the temperature of transition to the absorptive state. In this regime, hydrogen is heated directly by bulk absorption of laser energy, and this delocalization of heat energy compared to absorption at the foil surface limits the achievable temperature, producing the plateau effect.

Transient absorption measurements (Fig. 2) confirm the change in thermal history is correlated with increased optical absorption. Here, absorption coefficient $\alpha = -\ln(I_H/I_C)/d$, where d is the thickness of the hot region (estimated from FE calculations, and of order 1 μm at 141 GPa), while I_C and I_H are transmitted probe intensities through cold and hot samples, respectively. Peak α near 1 μm^{-1} are consistently inferred, with total uncertainty of about an order of magnitude largely due to thickness uncertainty and reproducibility.

To compare our optical measurements in a wide, previously unexplored region of the phase diagram to prior data, we interpolated direct-current (DC) conductivity (σ_0) measurements on fluid hydrogen [3,11,12,29,40] using an experimentally-consistent model [34] having the form $\sigma^* = \sigma_m^* - \sigma_j^*\{1 - 0.5\,\mathrm{erfc}[(T^* - T_c^*)/T_w^*]\}$,

where $\sigma^* = \log(\sigma_0)$ and $T^* = 1/T$. This model has a sigmoidal temperature dependence that reproduces the Arrhenius- or semiconductor-like proportionality of $\sigma^* \propto T^*$ during the IMT [11,12,29], with constant conductivity in purely metallic (σ_m^*) [13,14,29] and insulating ($\sigma_m^* - \sigma_j^*$) [40] states; the transition temperature (T_c^*) and width (T_w^*) were taken to vary linearly with density [34].

Absorption spectra at 141 GPa and 2,400 K show increasing absorption with photon energy across the visible (Fig. 4a). Semiconductor-like absorption is one possible explanation: electronic band gaps on the order of the present optical energies have been reported in dense hydrogen [3,8,9,12,16,29,41,42]. The data do not permit the exact assignment to existing semiconductor or semi-metal models. However, given the disordered nature of the material and rather large values of the absorption coefficients (up to ~10^6 m^{-1}), we suggest that observed absorption is due to optical processes between extended states, which are well described by Tauc's relation $\alpha = A(\hbar\omega - E_g)^2/\hbar\omega$. This well fits the data, implying a gap E_g of 0.9±0.3 eV. In this semiconductor picture, hydrogen is electrically conductive due to thermal excitation of electrons. Assuming an effective carrier mass of 0.5-1 m_e [13,33] the DC conductivity at these conditions is predicted to be 5-23 S/cm for E_g=0.9 eV, in agreement with that determined from shock data (~15 S/cm) [43]. The spectral character is consistent with theory for semiconducting hydrogen at similar pressure and lower temperature [16] which may be similarly described by the Tauc model.

Conductivity at optical frequencies is $\sigma = n\alpha c\varepsilon_0$, where n is the real index of refraction [44,45] which is weakly dependent on material properties, and always of order 10^0 [34]. Thus, σ is determined principally by α, which varies by many orders of magnitude during electronic transformation. The conductivity at 2400 K and 141 GPa varies between ~70 and ~220 S/cm from 1.55 to 2.3 eV, and this extrapolated to

zero energy is consistent with the DC conductivity of ~15 S/cm (Fig. 4b). The decrease in conductivity with energy is inconsistent with the simple Drude model of free carriers widely used for hydrogen at extreme conditions [2,11-14,16,17].

A modified Drude model, after Smith [46], given by $\sigma = \sigma_0[1 + C\ (1 - \omega^2\tau^2)/(1 + \omega^2\tau^2)]/[(1 + C)(1 + \omega^2\tau^2)]$ and incorporating reduced electron mobility through a backscattering term *C*, does provide an adequate representation of the data including the DC limit (Fig. 4b). This model has features typically observed in poor metals at the boundary of metallization transitions such as mercury [46] and argon [33], suggesting its applicability for hydrogen at the IMT. The parameter *C*, a measure of how closely the spectrum follows the Drude (free-electron) approximation, ranges from 0 to -1, with $C = 0$ (minimum backscattering) corresponding to the Drude form. Fits to our data show *C* is closer to -1 at conditions of incipient metallization (Fig. 4c). This is consistent with theories for conducting hydrogen [17,21,23,24], which are well described by a Smith-Drude model with $C \neq 0$ [34]. Scattering times τ from Smith-Drude fits are insensitive to pressure and temperature (Fig. 4d) despite conditions sampled by experiment and theory ranging from 24-6,000 GPa, 1,000-125,000 K, and 0.3-5.4 g/cc in pressure, temperature, and density, respectively [17,21,23,24], and are consistent with the expected minimum scattering time (Ioffe-Regal limit) [12,13] where scattering occurs at the interatomic spacing. Conductivity peaks at $\omega_m \approx 1/\tau$ when $C \approx -1$, or $\hbar\omega_m \approx 10$ eV for the present data. The fact that conduction is maximized in conjunction with the shortest-distance carrier motion possible indicates that transport is dominated by motion of bound carriers, such as hopping [18], as opposed to unimpeded long-distance flow.

The temperature at which absorbing hydrogen appears (at detection limit $\alpha \approx 0.1\ \mu m^{-1}$) decreases weakly with pressure, remaining at 1700-2500 K at 30-110 GPa

(Fig. 1). Here $\sigma_0 \approx 10^{-3}$ S/cm, which is below the optical conductivity, $\sigma \approx 10^0$ S/cm. The data at 141 GPa and 2400 K have $\sigma_0 \sim 10^1$ S/cm, and $\sigma \sim 10^2$ S/cm at visible frequencies (Fig. 4b). Fluid hydrogen thus shows optical properties characteristic of a weak metal [17,21,23,24] and a semiconductor undergoing gap closure [16] (σ increasing with frequency) throughout the observed pressure range at temperatures of 1700-2500 K. Measured optical conductivities (Fig. 4) are less than those of the metallic state (~2000 S/cm) [12,29], whereas optical reflectivity R, estimated by assessing the Fresnel reflectivity between insulating (cold) and optically transformed (hot) states in the experiment, is $R \sim [(4n\omega/\alpha c)^2 + 1]^{-1}$ or less than ~1% at presently examined conditions.

Our data directly show hot fluid hydrogen retains a significant band gap to above 140 GPa pressure (Fig. 4) and temperatures of 2000-3000 K. Prior interpretations of conductivity data, assuming a density-dependent, temperature-independent gap, predicted metallization at these conditions (densities above 0.32 mol-H_2/cc) via compressive gap closure [3,12,29]. The difference between our direct measurement and the prior model result is attributed to temperature dependence of the gap. Indeed, the temperature at which absorption appears in fluid hydrogen is nearly density- and pressure-independent between 30 – 110 GPa, suggesting gap closure is primarily thermal rather than compressive.

Our definitive observation of a weakly conducting, semiconductor-like state of hot fluid hydrogen in measurements to 150 GPa rules out the possibility of a rapid or first-order transformation between insulator and metal at these pressures. This is inconsistent with some *ab-initio* theoretical predictions [5,19,21,22] and supports more recent theories employing nonlocal density functionals and nuclear quantum effects [25] or quantum Monte Carlo molecular dynamics [27], which place a critical

196 point at 250-375 GPa. Isentropic compression measurements find the IMT becomes
197 first order by 285 GPa [16], suggesting together with our results an experimental
198 critical point between 150 and 285 GPa. Also, the gap in temperature between
199 insulating and metallic conditions appears to be decreasing with pressure in the
200 studied range, consistent with the transition sharpening towards a critical point at
201 higher pressures (Fig. 1): at 22 GPa, reflectivity [14] onsets 3710 K above absorption;
202 at 45 GPa, the difference is 1540 K). Parallel behavior is seen in the DC conductivity
203 (Fig. 1).

204 Prevailing first-principles models for hydrogen and hydrogen-bearing systems
205 at high pressure and temperature in giant planets [4,5,47] thus require a significant
206 reassessment. Compared with these theories, metallic conditions occur at higher
207 pressure and temperature (i.e. deeper within the planets), potentially influencing
208 atmospheric coupling with the metallic layer [6,7] and the conditions of hydrogen-
209 helium phase separation. For example, as conditions of phase separation are
210 correlated with the location of the critical point [4,5,47], the increased pressure of the
211 critical point required by our direct observations to 150 GPa suggests phase separation
212 is unlikely to have occurred in Jupiter [34].

213 Our optical properties measurements on hydrogen cover a wide, previously
214 unexplored region of the phase diagram and bridge large gaps between prior dynamic
215 and static compression measurements of transformation and transport properties. Our
216 data show the presence of an intermediate absorptive but not metallic state of
217 hydrogen at the boundary between insulating and metallic regimes in a wide pressure
218 range (10-150 GPa). This is inconsistent with first-order insulator-metal transition and
219 compression-driven gap closure that were previously inferred in this region from
220 experiments and theory.

We thank S. Lobanov and M. Ahart for experimental assistance, C.T. Seagle, R. Boehler, and R.J. Hemley for helpful discussions, and R.T. Howie, V. Struzhkin, E. Gregoryanz, and two anonymous reviewers for constructive suggestions on this manuscript. This work was supported by the NSF Major Research Instrumentation program, NSF EAR-1015239, NSF EAR-1520648 and NSF EAR/IF-1128867, the Army Research Office (56122-CH-H), the Carnegie Institution of Washington, the Deep Carbon Observatory Instrumentation grant, the British Council Researcher Links programme, the DOE NNSA Carnegie/DOE Alliance Center (DE-FC52-08NA28554), the DOE EFRC for Energy Frontier Research in Extreme Environments (EFREE), and NSFC (No. 21473211).

231 FIGURE CAPTIONS

232

233 FIG. 1. (color) Phase diagram of hydrogen. Black lines are phase boundaries. Present
234 measurements are filled circles for transparent (white), and absorbing (grey, black)
235 hydrogen; black points are characterized via direct transient absorption measurement
236 (Fig. 2) whereas grey points correspond to anomalous temperature responses observed
237 upon increasing heating laser power (Fig. 3). A thermal pressure of 2.5 GPa/1000 K
238 [48] is included. The heavy black line is onset of absorbing hydrogen in the present
239 data. Prior measurements are the onset of reflectivity in shock compression [14]
240 (crosses and dotted line), the onset of visible absorption in isentropic compression
241 [16] (squares and dashed line), the location of anomalies in temperature with
242 increasing heating laser power in the DAC [15] (stars), and the DC conductivity
243 (color map) based on interpolated data [3,11,12,29,34,40]. The melting curve is taken
244 from Ref. [28] and the metallization line is the saturation of DC conductivity. White
245 lines are interior conditions of Jupiter [49] and Saturn [50].

246

247 FIG. 2. (color) Transient absorption and emission measurements in hydrogen at 141
248 GPa. (a) Laser power (upper panel) and spectrogram showing transient absorption
249 (lower panel). (b) Time histories of absorption at different wavelengths using pulse
250 referencing [33,34]. (c) Transmission spectrum averaged over 2 to 5 μs where
251 absorption (and temperature) is roughly constant. (d) Emission spectrogram (20
252 spectrograms stacked), with inset showing gray-body Planck fit to data at 2 to 5 μs.
253 Temperature in this time interval was 2400(300) in a series of heat cycles at this laser
254 power.

255

256 FIG. 3. (color) Temperature histories at 30 GPa with finite element model predictions.
257 Two measurements (open symbols: vertical bars are temperature uncertainty,
258 horizontal bars are time resolution) are presented with finite element models
259 [33,34,39] with and without an onset of infrared absorption in hydrogen at a critical
260 temperature of ~3300 K (solid and dashed lines, respectively). Below the critical
261 temperature (blue points), models (grey) are indistinguishable and follow behavior
262 typical for a transparent sample with laser energy absorption on the foil surface [39].
263 For experiments achieving the critical temperature (red points), models (black) show
264 the result of sample absorption: rather than an initial peak and decay that scaled with
265 laser power, temperature is limited to values near the critical temperature [33]. Laser
266 power increased from 65 to 155 W between the models. Above 100 GPa transient
267 absorption occurred without this effect, since thinner samples at high pressure did not
268 become infrared-optically thick when heated.
269
270 FIG. 4. Optical properties of hydrogen. Data at 141 GPa and 2400(300) K are open
271 circles (error bars are systematic), theoretical predictions are crosses, and fits are
272 lines. (a) Absorption spectra with Tauc fits, with theory for semiconducting states at
273 1600-1700 K, 101-159 GPa [16]. (b) Conductivity spectra with Smith-Drude fits. The
274 DC conductivity corresponding to the present data and used in the fitting is $\sigma_0 = 15$
275 S/cm (triangle). Theory for metal and nonmetal states are for 1000 K, 170 GPa [21].
276 (c) Smith-Drude backscattering parameter *C* and (d) scattering time τ are from theory
277 [17,21,23,24,34] and experiment; shaded region in (c) is the conditions for
278 metallization [12,21,29] and in (d) the calculated minimum scattering time (Ioffe-
279 Regal limit) [12,13] for relevant conditions.
280

281

FIGURES

FIG. 1

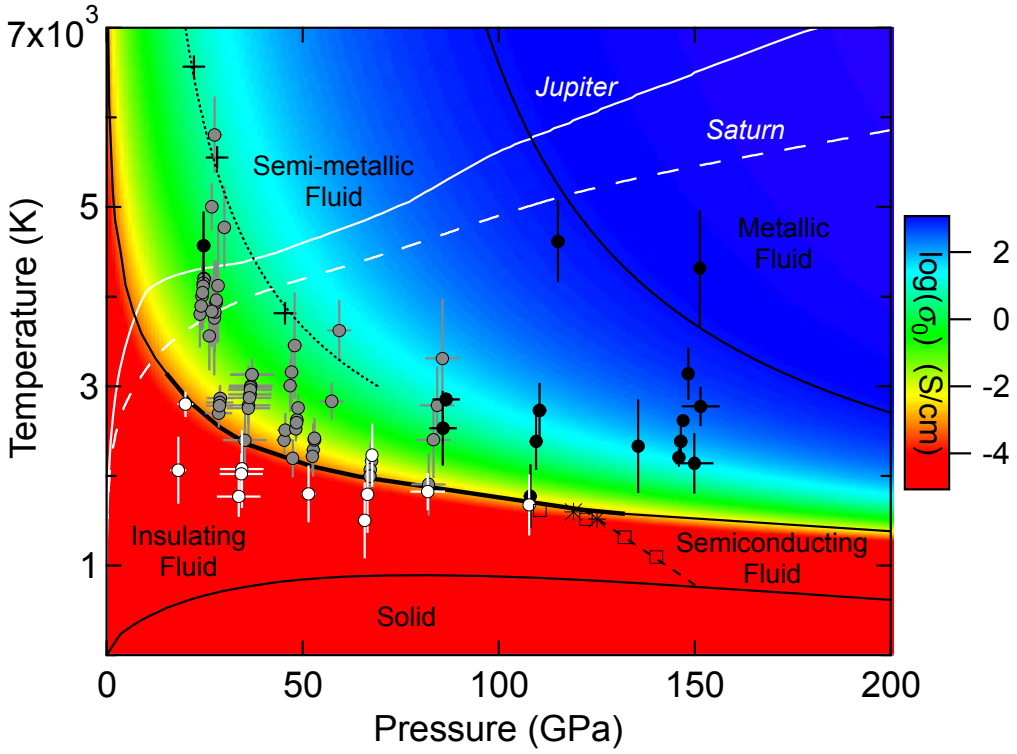

FIG. 2

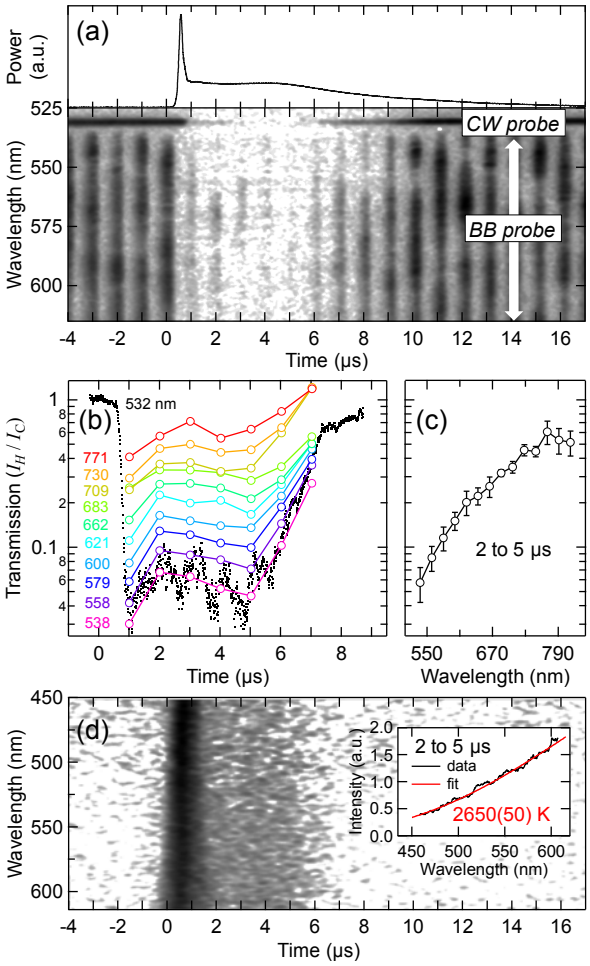
(a)
Power (a.u.)
525
550
575
600
Wavelength (nm)
CW probe
BB probe
-4 -2 0 2 4 6 8 10 12 14 16
Time (μs)
(b)
532 nm
771
730
709
683
662
621
600
579
558
538
Transmission (I_H / I_C)
1
0.1
0 2 4 6 8
Time (μs)
(c)
2 to 5 μs
550 670 790
Wavelength (nm)
(d)
450
500
550
600
Wavelength (nm)
-4 -2 0 2 4 6 8 10 12 14 16
Time (μs)
2 to 5 μs
data
fit
2650(50) K
Intensity (a.u.)
2.0
1.5
1.0
0.5
0.0
450 500 550 600
Wavelength (nm)

FIG. 3

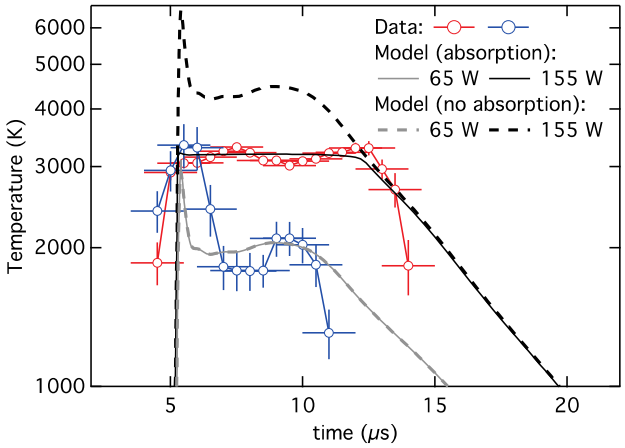
Data:
Model (absorption):
65 W
155 W
Model (no absorption):
65 W
155 W
Temperature (K)
6000
5000
4000
3000
2000
1000
5
10
15
20
time (μs)

FIG. 4

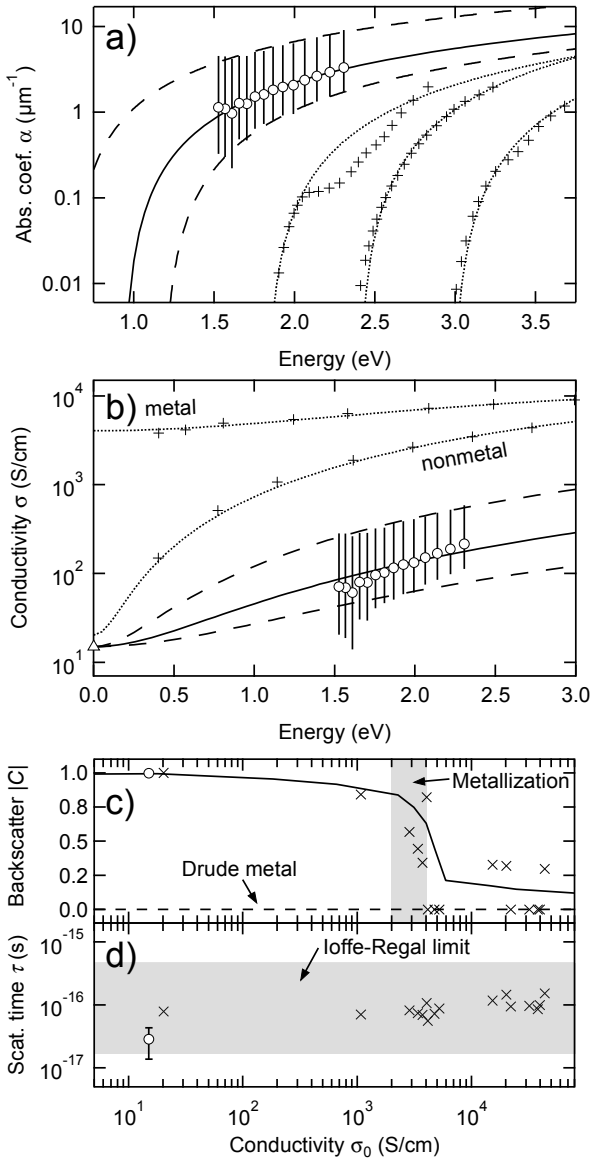
a)
Abs. coef. α (μm^-1)
10
1
0.1
0.01
1.0
1.5
2.0
2.5
3.0
3.5
Energy (eV)
b) metal
nonmetal
Conductivity σ (S/cm)
10^4
10^3
10^2
10^1
0.0
0.5
1.0
1.5
2.0
2.5
3.0
Energy (eV)
c)
Backscatter |C|
1.0
0.8
0.5
0.2
0.0
Metallization
Drude metal
d)
Scat. time τ (s)
10^-15
10^-16
10^-17
Ioffe-Regal limit
10^1
10^2
10^3
10^4
Conductivity σ0 (S/cm)

309 REFERENCES
310
311

312 [1] N. W. Ashcroft, Physical Review Letters **21**, 1748 (1968).
313 [2] S. X. Hu, L. A. Collins, V. N. Goncharov, T. R. Boehly, R. Epstein, R. L.
314 McCrory, and S. Skupsky, Physical Review E **90**, 033111 (2014).
315 [3] W. J. Nellis, S. T. Weir, and A. C. Mitchell, Science **273**, 936 (1996).
316 [4] W. Lorenzen, B. Holst, and R. Redmer, Physical Review Letters **102** (2009).
317 [5] W. Lorenzen, B. Holst, and R. Redmer, Physical Review B **84**, 7, 235109
318 (2011).
319 [6] M. Heimpel and N. Gómez Pérez, Geophysical Research Letters **38** (2011).
320 [7] T. Gastine, J. Wicht, L. D. V. Duarte, M. Heimpel, and A. Becker,
321 Geophysical Research Letters **41**, 5410 (2014).
322 [8] P. Loubeyre, F. Occelli, and R. LeToullec, Nature **416**, 613 (2002).
323 [9] R. T. Howie, C. L. Guillaume, T. Scheler, A. F. Goncharov, and E.
324 Gregoryanz, Physical Review Letters **108**, 125501 (2012).
325 [10] C.-s. Zha, Z. Liu, M. Ahart, R. Boehler, and R. J. Hemley, Physical Review
326 Letters **110**, 217402 (2013).
327 [11] W. J. Nellis, A. C. Mitchell, P. C. McCandless, D. J. Erskine, and S. T. Weir,
328 Physical Review Letters **68**, 2937 (1992).
329 [12] W. J. Nellis, S. T. Weir, and A. C. Mitchell, Physical Review B **59**, 3434
330 (1999).
331 [13] P. M. Celliers, G. W. Collins, L. B. Da Silva, D. M. Gold, R. Cauble, R. J.
332 Wallace, M. E. Foord, and B. A. Hammel, Physical Review Letters **84**, 5564 (2000).
333 [14] P. Loubeyre, S. Brygoo, J. Eggert, P. M. Celliers, D. K. Spaulding, J. R. Rygg,
334 T. R. Boehly, G. W. Collins, and R. Jeanloz, Physical Review B **86**, 9, 144115 (2012).
335 [15] V. Dzyabura, M. Zaghoo, and I. F. Silvera, Proc. Natl. Acad. Sci. U. S. A.
336 **110**, 8040 (2013).
337 [16] M. D. Knudson, M. P. Desjarlais, A. Becker, R. W. Lemke, K. R. Cochrane,
338 M. E. Savage, D. E. Bliss, T. R. Mattsson, and R. Redmer, Science **348**, 1455 (2015).
339 [17] L. A. Collins, S. R. Bickham, J. D. Kress, S. Mazevet, T. J. Lenosky, N. J.
340 Troullier, and W. Windl, Physical Review B **63**, 11, 184110 (2001).
341 [18] R. Redmer, G. Röpke, S. Kuhlbrodt, and H. Reinholz, Physical Review B **63**,
342 233104 (2001).
343 [19] S. Scandolo, Proceedings of the National Academy of Sciences **100**, 3051
344 (2003).
345 [20] S. A. Bonev, E. Schwegler, T. Ogitsu, and G. Galli, Nature **431**, 669 (2004).
346 [21] M. A. Morales, C. Pierleoni, E. Schwegler, and D. M. Ceperley, Proc. Natl.
347 Acad. Sci. U. S. A. **107**, 12799 (2010).
348 [22] I. Tamblyn and S. A. Bonev, Physical Review Letters **104**, 4 (2010).
349 [23] S. Hamel, M. A. Morales, and E. Schwegler, Physical Review B **84**, 165110
350 (2011).
351 [24] L. A. Collins, J. D. Kress, and D. E. Hanson, Physical Review B **85**, 233101
352 (2012).
353 [25] M. A. Morales, J. M. McMahon, C. Pierleoni, and D. M. Ceperley, Physical
354 Review Letters **110**, 065702 (2013).
355 [26] G. Mazzola, S. Yunoki, and S. Sorella, Nat Commun **5** (2014).
356 [27] G. Mazzola and S. Sorella, Physical Review Letters **114**, 105701 (2015).

[28] R. T. Howie, P. Dalladay-Simpson, and E. Gregoryanz, Nat Mater **14**, 495 (2015).
[29] S. T. Weir, A. C. Mitchell, and W. J. Nellis, Physical Review Letters **76**, 1860 (1996).
[30] J. H. Eggert, D. G. Hicks, P. M. Celliers, D. K. Bradley, R. S. McWilliams, R. Jeanloz, J. E. Miller, T. R. Boehly, and G. W. Collins, Nature Physics **6**, 40 (2010).
[31] N. Subramanian, A. F. Goncharov, V. V. Struzhkin, M. Somayazulu, and R. J. Hemley, Proc. Natl. Acad. Sci. U. S. A. **108**, 6014 (2011).
[32] A. F. Goncharov and J. C. Crowhurst, Physical Review Letters **96**, 4, 055504 (2006).
[33] R. S. McWilliams, D. A. Dalton, Z. Konopkova, M. F. Mahmood, and A. F. Goncharov, Proceedings of the National Academy of Sciences **112**, 7925 (2015).
[34] *See Supplemental Material at [URL will be inserted by publisher] for supporting figures and data.*
[35] H. K. Mao and R. J. Hemley, Reviews of Modern Physics **66**, 671 (1994).
[36] Y. Akahama and H. Kawamura, High Pressure Research **27**, 473 (2007).
[37] H. K. Mao, J. Xu, and P. M. Bell, Journal of Geophysical Research-Solid Earth and Planets **91**, 4673 (1986).
[38] T. Scheler, M. Marques, Z. Konopkova, C. L. Guillaume, R. T. Howie, and E. Gregoryanz, Physical Review Letters **111**, 5, 215503 (2013).
[39] J. A. Montoya and A. F. Goncharov, J. Appl. Phys. **111**, 9 (2012).
[40] W. L. Willis, Cryogenics **6**, 279 (1966).
[41] C.-S. Zha, Z. Liu, and R. J. Hemley, Physical Review Letters **108**, 146402 (2012).
[42] A. F. Goncharov, J. S. Tse, H. Wang, J. Yang, V. V. Struzhkin, R. T. Howie, and E. Gregoryanz, Physical Review B **87**, 024101 (2013).
[43] DC conductivity is taken from the lower end of the temperature range achieved at this laser power, since the stacked transient absorption data (Fig. 2) is dominated by those cycles reaching lower temperature and lower absorption.
[44] W. J. Evans and I. F. Silvera, Physical Review B **57**, 14105 (1998).
[45] R. J. Hemley, M. Hanfland, and H. K. Mao, Nature **350**, 488 (1991).
[46] N. V. Smith, Physical Review B **64**, 155106 (2001).
[47] M. A. Morales, S. Hamel, K. Caspersen, and E. Schwegler, Physical Review B **87**, 4, 174105 (2013).
[48] A. F. Goncharov, J. C. Crowhurst, J. K. Dewhurst, S. Sharma, C. Sanloup, E. Gregoryanz, N. Guignot, and M. Mezouar, Physical Review B **75**, 224114 (2007).
[49] N. Nettelmann, A. Becker, B. Holst, and R. Redmer, Astrophys. J. **750**, 10, 52 (2012).
[50] N. Nettelmann, R. Pustow, and R. Redmer, Icarus **225**, 548 (2013).
[51] R. J. Hemley, H. K. Mao, L. W. Finger, A. P. Jephcoat, R. M. Hazen, and C. S. Zha, Physical Review B **42**, 6458 (1990).